Published in final edited form as:

FASEB J. 2020 May ; 34(5): 6369–6381. doi:10.1096/fj.201902611R.

Genetic interaction of mammalian IFT-A paralogs regulates cilia disassembly, ciliary entry of membrane protein, Hedgehog signaling and embryogenesis

Wei Wang[1], **Bailey A. Allard**[1], **Tana S. Pottorf**[1], **Henry H. Wang**[1], **Jay L. Vivian**[2], **Pamela V. Tran**[1]

[1]Department of Anatomy and Cell Biology, Jared Grantham Kidney Institute, University of Kansas Medical Center, Kansas City, KS

[2]Department of Pathology and Laboratory Medicine, University of Kansas Medical Center, Kansas City, KS

Abstract

Primary cilia are sensory organelles that are essential for eukaryotic development and health. These antenna-like structures are synthesized by intraflagellar transport protein complexes, IFT-B and IFT-A, which mediate bi-directional protein trafficking along the ciliary axoneme. Here using mouse embryonic fibroblasts (MEF), we investigate the ciliary roles of two mammalian orthologues of *Chlamydomonas* IFT-A gene, *IFT139*, namely *Thm1* (also known as *Ttc21b*) and *Thm2 (Ttc21a). Thm1* loss causes perinatal lethality, and *Thm2* loss allows survival into adulthood. At E14.5, the number of *Thm1;Thm2* double mutant embryos is lower than that for a Mendelian ratio, indicating deletion of *Thm1* and *Thm2* causes mid-gestational lethality. We examined the ciliary phenotypes of mutant MEF. *Thm1*-mutant MEF show decreased cilia assembly, increased cilia disassembly, shortened primary cilia, a retrograde IFT defect for IFT and BBS proteins, and reduced ciliary entry of membrane-associated proteins. *Thm1*-mutant cilia also show a retrograde transport defect for the Hedgehog transducer, Smoothened, and an impaired response to Smoothened agonist, SAG. *Thm2*-null MEF show normal ciliary dynamics and Hedgehog signaling, but additional loss of a *Thm1* allele impairs response to SAG. Further, *Thm1;Thm2* double mutant MEF show enhanced cilia disassembly, and increased impairment of INPP5E ciliary import. Thus, *Thm1* and *Thm2* have unique and redundant roles in MEF. *Thm1* regulates cilia assembly, and alone and together with *Thm2*, regulates cilia disassembly, ciliary entry of membrane-associated protein, Hedgehog signaling, and embryogenesis. These findings shed light on mechanisms underlying *Thm1*-, *Thm2*- or IFT-A-mediated ciliopathies.

Keywords

primary cilia; development; mouse model; mouse embryonic fibroblasts

*Correspondence should be addressed to: Pamela V. Tran, Department of Anatomy and Cell Biology and The Jared Grantham Kidney Institute, University of Kansas Medical Center, 3901 Rainbow Blvd., MS #3038, Kansas City, KS 66160, Tel: 913-945-7325, Fax: 913-588-2710, ptran@kumc.edu.

Author Contributions

WW, BAA, TSP and HHW performed experiments. WW, BAA, TSP, HHW, JLV and PVT analyzed data. WW, JLV and PVT designed research. TSP generated model. WW and PVT wrote the paper.

Introduction

Cilia are evolutionarily-conserved organelles present in most eukaryotic organisms from *Chlamydomonas reinhardtii* to vertebrates (1). These microtubular organelles can confer motility or act as sensory organelles. In the latter role, a singular cilium, termed a primary cilium, extends from the apical surface of a cell, where it detects and transduces extracellular signals. Primary cilia regulate cell cycle, cell differentiation and cell-cell communication (2).

Mutations that disrupt cilia function cause multi-system disorders, termed ciliopathies (3). Clinical manifestations can include craniofacial and neural tube defects, retinal degeneration, skeletal dysplasia, fibrocystic diseases of the kidney, liver, and pancreas, obesity, and male infertility (4). Understanding the role of ciliary proteins in mediating ciliary processes can provide insight into cellular mechanisms underlying these various defects.

The primary cilium consists of a microtubule-based ciliary axoneme, ensheathed in a ciliary membrane. Extension and maintenance of the axoneme is dependent on multiple protein complexes (5). The IFT-B complex, comprised of approximately 15 proteins, and the kinesin motor mediate anterograde transport, moving protein cargo from the base to the tip of the primary cilium. The IFT-A complex, comprised of approximately 7 proteins, together with the dynein motor mediate retrograde transport, returning cargo from the tip to the base of the primary cilium. IFT-A proteins also mediate ciliary entry of signaling and membrane-associated proteins (6–8). Another protein complex, the BBSome, traffics signaling molecules to the cilium and throughout the cilium where it acts as an adaptor between the IFT complexes and the protein cargoes(9). Despite that these ciliary proteins assemble into complexes, mutations in ciliary genes that encode proteins of the same ciliary complex can result in different phenotypes (10). Thus, individual ciliary proteins likely have cell-specific roles.

Previously, we identified the mammalian IFT-A gene, *Thm1* (TPR-containing Hedgehog Modulator 1; also known as *Ttc21b*), an orthologue of *Chlamydomonas reinhardtii fla17/ift139* (11, 12). In mouse, early embryonic loss of *Thm1* misregulates Hedgehog (Hh) signaling and causes perinatal lethality, polydactyly, and defects of the skeleton, forebrain, palate, and neural tube (11, 13, 14). Additionally, in mice, *Thm1* deletion in the perinatal period causes renal cystic disease (15), and its deletion in adulthood causes obesity (16). These phenotypes recapitulate the clinical features present in individuals with ciliopathies who have *THM1* mutations. Causative mutations in *THM1* have been identified in patients with nephronophthisis, a renal fibrocystic disease, while modifying mutations in *THM1* have been found in patients with Bardet Biedl Syndrome, which manifests obesity as a cardinal clinical feature (17).

Loss or deficiency of *Thm1* impairs retrograde IFT, resulting in accumulation of IFT proteins and signaling molecules at the ciliary distal tip (11, 18). In some cells, such as mesenchymal cells of the developing limb bud, *Thm1* depletion causes shortened cilia (11), while in cultured RPE cells, cilia length was not affected (18). In *Chlamydomonas ift139-*

null mutants, levels of other IFT-A proteins were reduced, indicating that in the green alga, IFT139 is required for assembly of the IFT-A complex (19).

While there is only one *ift139* gene in *Chlamydomonas*, evolution has generated two vertebrate orthologues, which we have called *Thm1* and *Thm2*. THM1 and THM2 proteins are both 50% identical to *Chlamydomonas* IFT139 (11, 12). Additionally, the murine *Thm1* and *Thm2* sequences are 50% homologous and encode proteins that have very similar predicted protein structures with multiple (10–11) tetratricopeptide repeat (TPR) domains. At embryonic day (E) 10.5, *Thm1* and *Thm2* also show very similar RNA expression patterns in whole mouse embryos. Recently, *THM2* mutations were identified in adult males with subfertility, and *Thm2* knock-out male mice have been reported to be subfertile (20). Still the role of *Thm2* in ciliogenesis and development remains uncharacterized. By generating a *Thm2*-null mouse and using *Thm1*- and *Thm2*-null derived mouse embryonic fibroblasts (MEF), here we show a role for *Thm1* in cilia assembly, and an interaction between *Thm1* and *Thm2* in cilia disassembly, ciliary entry of membrane-associated protein, Hh signaling and embryogenesis.

Materials and Methods

Generation of Thm2 knockout (Thm2$^{-/-}$) mouse

Thm2-null mice were generated using CRISPR/Cas9 genome editing. Two guide RNAs (gRNAs) – one targeting exon 4 (target sequence CATACTCCCTGGCCTTGTCGTGG) and the other in intron 8 (target sequence AACCTGACCGACAGCCCACCTGG) - were designed to delete exons 4–8 and ultimately cause a premature stop codon. gRNAs were generated and validated by the Washington University Genome Engineering and iPSC Center). Pro-nuclear injections of 20ng/μl of each in vitro transcribed gRNA and 50ng/μl of Cas9 mRNA of 317 F1 embryos derived from FVB oocyte donors and C57BL6/J males yielded 42 founders. Genomic DNA of founders was amplified and sequenced to determine presence of exon 4–8 deletion and a resulting premature stop codon. Founders carrying a large deletion and stop codon were then crossed to FVB mice to expand the *Thm2*$^{-/-}$ lines.

Genotyping of NHEJ events following CRISPR/Cas9 genome editing

Three PCR primer sets were designed to characterize the deletions generated by non-homologous end joining (NHEJ) following CRISPR/Cas9 genome editing. Two sets of primers were designed around the exon 4 gRNA, and one set of primers was designed to flank the entire region between exon 4 and intron 8. The first primer set surrounding exon 4 included F-Thm2ex4p (5’-TAC TAC GCC AGC CTC TTC CT- 3’) and R-Thm2ex4p (5’-CCC TCC TGT ACC TCT TTG GA-3’) and was expected to produce a WT band of 107bp. The second primer set surrounding exon 4 included F-Thm2ex4r (5’- TGT CTG AAG CCA ACA GAG AGG-3’) and R–Thm2ex4r (5’-GTT CAA GGC CAC CTT TGC T-3’) and was expected to produce a WT band of 1,000bp. PCR amplicons with a lower molecular weight indicate evidence of NHEJ in exon 4. Primers designed to detect the large exon 4–8 deletion flank exon 4 and intron 8 include F-Thm2ex4b (5’-GGA GAG CAG CTT GAA GGA AA-3’) and R-Thm2ex4b (5’-GTC ACG GCT GGT GTG ATT C-3’). A PCR amplicon was expected of approximately 216bp, only in the event of NHEJ. To detect the presence of a

WT allele, a separate PCR reaction was performed using primers within exon 6, F-WT (5-AAC TTC CTG CCC GCT TTA GT- 3') and R-WT (5'-GTG TCA GAT ACC CTG GAA CCA GAG-3'). In the presence of a WT allele, this PCR reaction yields an amplicon of approximately 461bp.

Sequencing of Thm2 knockout alleles

PCR products were run on an agarose gel, excised, and extracted using the Qiaex II DNA extraction kit (Qiagen, 20021). Samples were sequenced by Genewiz. Sequencing results were analyzed to determine the presence or absence of stop codons resulting from NHEJ events. A line harboring a deletion from exon 4 to intron 8, producing a stop codon in exon 4 was chosen, with the allele designation of *Ttc21a*$^{\Delta 4-8}$. The founder of this line was mated to FVB mice to expand the line. This line was maintained on the C57BL6/J/FVB mixed genetic background.

Analysis of mouse embryos and generation of mouse embryonic fibroblasts

Timed matings were performed between *Ttc21a*$^{\Delta 4-8/+}$; *Thm1*$^{aln/+}$ mice. The *aln* allele of *Thm1* results in absence of protein, and thus acts like a null allele (11). Visualization of a vaginal plug was designated as embryonic day (E) 0.5. Mouse embryos were dissected at E10.5, E12.5 and E14.5 using a Leica dissection microscope. Tails of mouse embryos were collected for genomic DNA extraction and genotyping. To generate MEF, embryos were eviscerated. In a fresh 10cm cell culture plate, an individual carcass was minced with a razor in 0.25% trypsin-EDTA, then media (DMEM containing 10% FBS and penicillin streptomycin antibiotics) was added. Cells were grown to confluency, then trypsinized and plated for an experiment. Cells were passaged maximally up to two times.

qPCR

RNA was extracted using Trizol (Life Technologies), then reverse transcribed into cDNA using Quanta Biosciences qScript cDNA mix (VWR International). qPCR for *Gli1* was performed using Quanta Biosciences Perfecta qPCR Supermix (VWR International) in a BioRad CFX Connect Real-Time PCR Detection System. Primers used were *mThm1* (Forward: 5'-AAGCTCAACCCTGACTTCTTAC-3'; Reverse: 5'-CAACGTCTGAGAACTGGAGAAA-3'), *mThm2* (Forward: 5'-CCCCACAATCCAAACCTACA-3'; Reverse: 5'-GCTCACAAGCCGATGGAC-3'), and m*Gli1* (Forward: 5'-CTGACTGTGCCCGAGAGTG-3'; Reverse: 5'-CGCTGCTGCAAGAGGACT-3'). qPCR was performed in duplicate using RNA lysates from three samples per genotype.

Cilia assembly and disassembly assays

Cells were plated on 12mm poly-L-lysine-coated coverslips in a 24-well plate with DMEM medium containing 10% FBS and pen/strep antibiotics. Two days after cells reached 100% confluency, medium was replaced with serum-free medium for 6 and 24 hours to assess early and late ciliogenesis, respectively. Cells were fixed, immunostained for ciliary markers, imaged and quantified for presence of cilia.

To measure cilia disassembly, cells were plated on 12mm poly-lysine coated glass coverslips in a 24-well plate with complete medium containing 10% FBS. Two days after cells reached 100% confluence, media was replaced with serum-free media for 24 hours to bring cells to G0 and induce ciliogenesis. Following 24-hour serum starvation, cells were cultured in media containing 10% FBS for 2 and 6 hours to induce cilia disassembly (21). Cells were fixed, immunostained for ciliary markers, imaged and quantified for presence of cilia.

Immunofluorescence

Cells were washed with PBS, then fixed with 4% paraformaldehyde/0.2% triton X-100 in PBS for 10 minutes at room temperature. Cells were washed again with PBS, and blocked with 1% BSA in PBS for 1 hour. Cells were then incubated with antibodies against SMO (Abcam), IFT52, IFT81, IFT88, IFT140, BBS2, BBS5 (Proteintech), ARL13B and INNP5E (Proteintech) and α-tubulin and acetylated α-tubulin (Sigma), and polyglutamylated tubulin (Adipogen) overnight at 4° C. Following 3 washes in PBS, cells were incubated with anti-rabbit AF488 and anti-mouse AF594 (InVitrogen Technologies) for 30 minutes at room temperature. Cells were washed 3X in PBS, and mounted with Vectashield containing 4,6-diamidino-2-phenylindole (DAPI) (Vector Laboratories). Immuno-labeled cells were viewed and imaged using a Leica TCS SPE confocal microscope configured on a DM550 Q upright microscope.

Results

Thm2 interacts with *Thm1* in embryogenesis

Timed matings of $Thm2^{\Delta 4-8/+};Thm1^{aln/+}$ intercrosses were performed. At E10.5, E12.5 and E14.5, pregnant females were dissected and their embryos analyzed. *Thm2*-null ($Thm2^{\Delta 4-8/\Delta 4-8}$) and *Thm2*-null; *Thm1*+/− ($Thm2^{\Delta 4-8/\Delta 4-8};Thm1^{aln/+}$) embryos were normal, while *Thm1*-null ($Thm1^{aln/aln}$) and *Thm1*; *Thm2* double knock-out ($Thm2^{\Delta 4-8/\Delta 4-8};Thm1^{aln/aln}$) embryos showed polydactyly and occasional exencephaly. At E10.5 and E12.5, the number of *Thm1*-null mutants and *Thm1; Thm2* double knock-outs (dko) was consistent with a Mendelian inheritance pattern, but at E14.5, the frequency of *Thm1; Thm2* dko embryos was reduced (Table 1). *Thm1* deletion causes perinatal lethality (11). Thus, the reduced number of *Thm1; Thm2* double mutants at E14.5 suggests that additional loss of *Thm2* exacerbates the *Thm1*-null developmental phenotype causing mid-gestational lethality.

Thm1 regulates ciliogenesis

We derived mouse embryonic fibroblasts (MEF) from E12.5 control, *Thm2* ko, *Thm2*-null; $Thm1^{+/-}$ (triple allele mutant), *Thm1*-null (ko), and *Thm1*; *Thm2* double-knockout (dko) mice. Using qPCR, we examined levels of *Thm1* and *Thm2* transcripts in control MEF and observed mean Cq values of 23 and 30, respectively (Figure S1A). Using serial dilutions of cDNA template made from MEF RNA for *Thm1* and testis RNA for *Thm2*, the R^2 value for both the *Thm1* and *Thm2* qPCR reactions was approximately 99%, indicating similar efficiency for the *Thm1* and *Thm2* qPCR reactions (Figure S1B). Therefore, the lower Cq values for *Thm1* indicate that *Thm1* is expressed at higher levels than *Thm2* in MEF. Further, *Thm2*-null MEF showed almost depleted levels of *Thm2* expression (Figure S1C).

Following 24 hours of serum starvation, *Thm1* ko cells exhibited shorter ciliary length (mean length of 3.5μm) than control cells (*Thm2*$^{+/-}$; mean length of 5.2μm), while the loss of *Thm2* did not alter cilia length (*Thm2*-null and *Thm2*-null;*Thm1*$^{+/-}$ mutants; mean lengths of 5.3μm and 5.2μm, respectively; Figures 1A and 1B).

We next assessed capacity of mutant cells to undergo ciliogenesis. At 6 and 24 hours of serum starvation, percentage of ciliated cells and cilia length was measured in control (*Thm2*$^{\Delta 4-8/+}$), *Thm2* ko (*Thm2*$^{\Delta 4-8/\Delta 4-8}$), triple allele mutant (*Thm2*$^{\Delta 4-8/\Delta 4-8}$;*Thm1*$^{aln/+}$), *Thm1* ko (*Thm1*$^{aln/aln}$) and *Thm1*; *Thm2* dko (*Thm1*$^{aln/aln}$; *Thm2*$^{\Delta 4-8/\Delta 4-8}$) MEF at 100% confluency. At 6 hours of serum starvation, approximately 75% of control MEF were ciliated. At 24 hours of serum starvation, percentage of ciliated control cells was not altered, but cilia length was increased (Figures 1C–1D). We posit that under our experimental conditions, early events in cilium formation, such as maturation and docking of the basal body, were completed at 6 hours of serum starvation, and that axoneme elongation occurred from 6 to 24 hours of serum starvation. In *Thm2* ko and in triple allele mutant MEF, percentage of ciliated cells and cilia lengths were similar to control MEF (Figure 1C, 1D, S2A, S2B). In contrast, percentage of ciliated *Thm1*-null MEF was lower than control MEF (48% vs. 75%, respectively) at 6 hours serum starvation, and increased (to 64%) at 24 hours of serum starvation, suggesting absence of *Thm1* reduces and delays ciliogenesis. From 6 to 24 hours serum starvation, cilia length did not change in *Thm1*-null MEF, suggesting that events required for axoneme elongation are hindered by *Thm1* loss. A similar percentage of ciliated cells and cilia length was observed in *Thm1;Thm2* dko MEF as in *Thm1*-null MEF, suggesting that *Thm2* does not participate in cilia assembly.

Thm2 interacts with *Thm1* to regulate cilia disassembly

Primary cilia undergo cycles of assembly and disassembly in coordination with the cell cycle, and the cilia assembly:disassembly ratio regulates cilia length (22, 23). To examine cilia disassembly, serum was added back to the media for 2 and 6 hours following 24 hours of serum starvation. After 2 hours of serum addition, percentage of ciliated control, *Thm2* ko, and triple allele mutant MEF was not significantly altered (approximately 78%), but cilia length was decreased (Figures 2A, 2B, S2C, S2D). In contrast, percentage of ciliated *Thm1*-null MEF reduced (63% vs. 55%) although this did not reach statistical significance, while cilia length was not altered. In *Thm1; Thm*2 dko MEF, 2 hour serum addition significantly reduced percent ciliated cells, but did not modify cilia length. These data suggest that the loss of *Thm1* and *Thm2* promotes cilia disassembly.

After 6 hours of serum addition, percentage of ciliated cells across all genotypes was significantly reduced (Figures 2A, 2B, S2C, S2D). Moreover, the decrease in percentage of ciliated cells from 24-hour serum starvation was greater in *Thm1*-null MEF than in control MEF (difference of 35% vs 19%), suggesting that *Thm1* loss alone increases cilia disassembly. In *Thm1; Thm*2 dko MEF, 6 hours of serum restimulation not only further reduced percentage of ciliated cells, but also decreased cilia length. Taken together, these results indicate that IFT-A deficiency promotes cilia disassembly.

Following 2 hours of serum addition, cells were immunostained for IFT-B protein, IFT81, and for acetylated α-tubulin. This revealed the presence of IFT81 that was separate and

distal to its axonemal localization (Figures 2C and S2C). To ensure that this IFT81 staining is truly distinct from the axoneme, cells were further immunostained for IFT81 together with α-tubulin or polyglutamylated tubulin. Similarly, IFT81 staining was observed that was separate and distal from tubulin (Figure S3). These observations may reflect the release of ciliary vesicles from the distal tip, a phenomenon that is termed decapitation or ectocytosis, and contributes to cilia disassembly (24). In *Thm1*-null and *Thm1*; *Thm2* dko cells, frequency of IFT81 localization that was separate from the axoneme was increased (Figure 2D; cilia + dot), suggesting *Thm1* regulates this phenomenon.

Thm1 regulates retrograde transport of IFT-B proteins

We next investigated the roles of *Thm1* and *Thm2* in ciliary protein transport. Following 24 hours of serum starvation to maximize cilia length, cells were immunostained for IFT-B subunits, IFT81 and IFT52, and for anterograde IFT motor, KIF3A. Ciliary localization of IFT-B proteins was similar between control, *Thm2* ko, and triple allele mutant MEF, while *Thm1*-null and *Thm1;Thm2* dko MEFs exhibited aberrant accumulation of proteins in a bulbous distal tip, indicative of defective retrograde IFT (Figures 3A–3C, S4). As described previously for IFT-A mutant cells (7), protein localization was classified as either absent in cilia (Cilia-), present in cilia without a bulb (Cilia w/o bulb), or present in cilia with a bulb (Cilia with bulb). Across all genotypes, virtually 100% of cilia showed the presence of IFT81, IFT52 and KIF3A. However, while most control, *Thm2* ko, and triple allele mutant MEF showed localization of IFT81, IFT52 and KIF3A in cilia without a bulb, approximately 50% of *Thm1*-null and *Thm1;Thm2* dko MEF showed localization of IFT81, IFT52 and KIF3A in a bulbous ciliary distal tip. *Thm1*; *Thm2* dko MEF displayed a slightly higher percentage of cells with IFT81 localizing to a ciliary bulbous distal tip than *Thm1*-null MEF (52% vs. 43%; Figure 3A). These data indicate that THM1 is required for retrograde transport of IFT-B proteins, and that THM2 may enhance THM1-mediated retrograde transport of IFT81.

Thm1 regulates ciliary entry and retrograde transport of IFT-A component, IFT140

We next examined ciliary localization of IFT-A component, IFT140. Approximately 80% −90% of cilia of control, *Thm2* ko, and triple allele mutant MEF showed the presence of IFT140, while only 65% of *Thm1*-null and *Thm1*; *Thm2* dko MEF had IFT140-positive cilia (Figures 4 and S4). To determine whether the reduction in ciliary IFT140 in *Thm1* and *Thm1;Thm2* mutant cells is due to reduced overall IFT140 protein levels, we immunoblotted whole cellular extracts for IFT140. Similar levels of IFT140 between control and the mutant genotypes were observed (Figure S5), indicating that unlike in *Chlamydomonas* (19), loss of *Thm1* in MEF does not affect IFT-A complex stability, and the reduction in ciliary IFT140 in *Thm1*-null and *Thm1;Thm2* dko MEF is due to a defect in ciliary entry. Additionally, approximately 35% of *Thm1*-null and *Thm1*; *Thm2* dko cilia showed IFT140 localization in a bulbous distal tip, indicative of a retrograde defect. Thus, THM1 mediates both ciliary entry and retrograde transport of an IFT-A protein.

Thm1 mediates retrograde transport of BBSome subunits

The BBSome is an 8-subunit complex, which acts like an adaptor between IFT complexes and protein cargo within cilia. BBSome subunits are normally rapidly exported from cilia (7,

25, 26). Consistent with this, we observed light ciliary staining of BBS2 in approximately 80% of control, *Thm2* ko, and triple allele mutant MEF (Figures 5A–5C, S4) and light ciliary staining of BBS5 in approximately 60% of control, *Thm2* ko, and triple allele mutant MEF (Figures 5D–5F, S4). However, approximately 95% of *Thm1*-null and *Thm1*; *Thm2* dko MEF showed ciliary presence of BBS2 and BBS5, and approximately 20% showed BBS2 and BBS5 localization in bulb-like structures at the distal tip (Figures 5B and 5E). *Thm1*-null and *Thm1*; *Thm2* dko cilia also showed increased intensity of BBS2 and BBS5 immunofluorescence relative to control cilia (Figures 5C and 5F). These data indicate that THM1 loss impairs retrograde IFT of the BBSome.

Thm2 interacts with *Thm1* to mediate ciliary localization of INPP5E

Since the IFT-A complex mediates ciliary entry of membrane-associated proteins (6–8), we next examined ciliary localization of ARL13B and INPP5E. While 100% of control, *Thm2* ko, and triple allele mutant MEF showed ciliary presence of ARL13B, approximately 90% of *Thm1*-null and *Thm1*; *Thm2* dko cilia were positive for ARL13B (Figures 6A, 6B, S4). Additionally, immunofluorescence intensity was decreased by almost 50% in *Thm1*-null and *Thm1*; *Thm2* dko cilia relative to control (Figure 6C). Further, while 95%−100% of control, *Thm2* ko, and triple allele mutant MEF showed ciliary presence of INPP5E, only 50% of *Thm1*-null MEF and 40% of *Thm1*; *Thm2* dko MEF had INPP5E-positive cilia (Figures 6D, 6E, S4). These data suggest *Thm1* regulates ciliary entry of ARL13B and INPP5E, and that *Thm2* enhances *Thm1*-mediated ciliary entry of INPP5E.

Thm2 interacts with *Thm1* to regulate Hh signaling

During activation of the mammalian Hedgehog (Hh) signaling pathway, the Smoothened (SMO) signal transducer enriches in the primary cilium (27). In control MEF, treatment with SMO agonist, SAG, resulted in presence of SMO in 60% of cilia, increased from 20% of cilia in untreated MEF (Figures 7A and 7B). Treatment with SAG also induced expression of *Gli1*, a transcriptional target and reporter of Hh activity (28). In triple allele mutant MEF, SAG treatment resulted in a ciliary enrichment of SMO similar to control cells (Figure 7B), yet *Gli1* expression was reduced relative to control MEF (Figure 7C). In contrast, SAG treatment of *Thm2* ko MEF induced similar levels of *Gli1* expression as control cells (Figure S6). In untreated *Thm1*-null and *Thm1*; *Thm2* dko MEF, SMO was present in 90% of cilia, and 20% showed SMO accumulation in a bulbous distal tip (Figure 7A). With SAG treatment, approximately 90% of cilia were SMO+, unchanged from untreated cells, but approximately 30% of cilia had SMO localized in a bulbous distal tip (Figure 7B). However, despite the increased presence of ciliary SMO in *Thm1*-null and *Thm1*; *Thm2* dko MEF, SAG-induced *Gli1* expression was minimal to almost absent (Figure 7C). Thus, these data show that *Thm1* regulates retrograde transport of SMO. These results are consistent with a previous study (18). Further, in MEF, *Thm1* is also required for Hh pathway activation downstream of SMO ciliary localization. Additionally, *Thm2* interacts with *Thm1*, to positively modulate Hh signaling downstream of SMO ciliary localization.

Discussion

In this study, we reveal that *Thm1* loss decreases cilia assembly, and that *Thm1* loss alone or together with *Thm2* loss, increases cilia disassembly. Since the ratio of cilia assembly:disassembly governs cilia length, this may account for the shorter cilia length in *Thm1*-null and *Thm1;Thm2* dko MEF. Further, in a *Thm1*-dependent manner, *Thm2* also regulates ciliary entry of membrane-associated protein, and Hh signaling activity downstream of SMO ciliary translocation (Figure 8).

This is the first demonstration of a role for IFT-A in cilia disassembly. In control MEF, two hours of serum restimulation following 24 hours of serum starvation did not alter percentage of ciliated cells, but decreased cilia length. Conversely, in *Thm1; Thm*2 dko cells, two hours of serum restimulation decreased percentage of ciliated cells, while cilia length was unchanged. This difference between control and mutant cells may indicate that in the presence of dysfunctional IFT-A, the mechanism of cilia disassembly is shifted. Several mechanisms contribute to cilia disassembly. These include cilia resorption, which gradually shortens cilia length; complete cilia shedding, which cleaves the entire cilium; and a combination of both mechanisms (29). The reduction in cilia length in control MEF suggests gradual cilia resorption may be a predominant mechanism within 2 hours of FBS stimulation, whereas the unaltered cilia length together with less ciliated *Thm1; Thm*2 dko MEF may suggest whole cilium shedding may predominate in these mutant cells during this time frame. Additionally, we observed increased frequency of IFT81 localization that was separate and distal to the ciliary axoneme in *Thm1*-null and *Thm1; Thm*2 dko cells after 2 hours of serum addition. This IFT81 localization may present decapitation or ectocytosis (24). The reduced ciliary INPP5E in *Thm1*-mutant and *Thm1; Thm*2 dko MEF could promote ectocytosis, since *Inpp5e*-null MEF have enhanced ectocytosis (24). Ectocytosis precedes cilia resorption (24), thus cilia resorption likely also occurs in *Thm1*-null and *Thm1; Thm*2 dko cells. In support of this, 2 and 6 hours of serum restimulation shortened primary cilia of *Thm1*-null and *Thm1; Thm*2 dko MEF, respectively. Further studies are required to determine the mechanisms by which IFT-A dysfunction regulates cilia disassembly.

The IFT-A complex can be subdivided into core and peripheral subcomplexes, comprised of IFT122/IFT140/IFT144 and of IFT42/IFT121/IFT139, respectively (18). Depletion of core versus peripheral subcomplex components has been shown to result in different phenotypes. For instance, *Ift144*-null RPE cells showed absence of SMO from cilia, suggesting defective ciliary import, while *Ift139*-null RPE cells accumulated SMO in cilia, indicating defective retrograde IFT (18). These contrasts may reflect differences in cargos carried by the subcomplexes or by the individual IFT-A proteins. *Thm1*-null MEF show ciliary protein trafficking defects similar to RPE cells depleted of peripheral subcomplex component, *Ift121/WDR35* (7). This includes defective retrograde transport of IFT and BBSome proteins, and impaired ciliary import of IFT-A protein, IFT140, and of membrane proteins, ARL13B and INPP5E. Similar also to IFT121/WDR35-depleted cells, *Thm1*-null MEF showed both reduced and delayed ciliogenesis. Reduced ciliary ARL13B in *Thm1*-null MEF may contribute to the reduced cilia assembly, since ARL13B is essential for ciliary membrane extension that is coupled to axoneme elongation (30). As a paralog of *Thm1*,

Thm2 is likely a component of the IFT-A peripheral subcomplex. However, the similar ciliary localization of IFT and BBS proteins in *Thm1* ko and *Thm1; Thm2* dko MEF suggest that majority of transport defects is due to loss of *Thm1*. This may be due to higher expression levels of *Thm1* than *Thm2* in MEF.

Although ciliary presence of SMO was increased in *Thm1*-null and *Thm1*; *Thm2* dko MEF, *Gli1* expression was not induced by SAG treatment, suggesting THM1 is required for Hh pathway activation downstream of SMO ciliary localization. This result was unexpected since we previously observed increased *Gli1* and *Ptch1* expression in E10.5 *Thm1*-null (*Thm1*$^{aln/aln}$) whole-mount mouse embryos, and ventralization of the neural tube of E9.5 and E10.5 *Thm1*-null embryos indicating enhanced activation of the Hh pathway (11). Two possibilities may explain this discrepancy. Additional signals or cell-cell interactions may be present *in vivo*, resulting in enhanced activation of the pathway during development. Alternatively, a study has demonstrated that *Thm1* can act as either a positive or negative regulator of Hh signaling in a cell-specific manner, since deletion of *Thm1* resulted in reduced Hh signaling in glial cells during cerebellum development (31). Similarly, other *Ift* genes have been shown to positively or negatively regulate the Hh pathway in a cell-type dependent manner (32). We observed that SAG-treated triple allele mutant MEF had reduced pathway activation relative to control cells, indicating that in a *Thm1*-dose dependent manner, *Thm2* positively regulates Hh signaling downstream of SMO ciliary localization in MEF. In this light, absence of Hh activation in *Thm1*-null cells is consistent with *Thm1* acting as a positive modulator of Hh signaling in MEF. The factors that determine whether an *Ift* gene positively or negatively regulates the Hh pathway are yet to be defined.

Pathogenic mutations of *THM1* have been identified in approximately 5% of patients with ciliopathies (17). Interestingly, one-third of patients with a homozygous mutation in another ciliary gene also harbored a heterozygote *Thm1* mutation, suggesting that *THM1* mutations can have causal or modifying effects in human ciliopathies. More recently, mutations in *THM2* were reported in male individuals with subfertility (20). Our studies reveal that *Thm2* interacts with *Thm1*, and thus identifying mutations in *THM2* and *THM1* in the same individual may warrant investigation. Our findings that *Thm1*, alone and/or together with *Thm2*, regulates ciliary entry of membrane protein, cilia assembly and disassembly, Hh signaling, and development, provide insight into potential mechanisms underlying IFT-A related ciliopathies.

Supplementary Material

Refer to Web version on PubMed Central for supplementary material.

Acknowledgements

We thank the KUMC Transgenic and Gene Targeting Institution Facility for generation of the *Thm2* mutant mice and acknowledge support of this Facility (Intellectual and Developmental Disabilities Research Center NIH U54 HD090216; KU Cancer Center NIH P30 CA168524; COBRE NIH P30 GM122731). This work was also supported by the National Institutes of Health [P30DK106912 to BAA]; [R01DK103033 to PVT].

Non-standard abbreviations

ARL13B	ADP Ribosylation Factor Like GTPase 13B
BBS	Bardet Biedl Syndrome
E	embryonic day
Hh	Hedgehog
INPP5E	Inositol Polyphosphate-5-Phosphatase E
IFT	intraflagellar transport
MEF	mouse embryonic fibroblasts
SAG	Smoothened agonist
SMO	Smoothened
Thm1	TPR-containing Hedgehog modulator 1
TPR	tetratricopeptide repeat

References

1. Plotnikova OV, Pugacheva EN, and Golemis EA (2009) Primary cilia and the cell cycle. Methods in cell biology 94, 137–160 [PubMed: 20362089]
2. Goetz SC, Ocbina PJ, and Anderson KV (2009) The primary cilium as a Hedgehog signal transduction machine. Methods in cell biology 94, 199–222 [PubMed: 20362092]
3. Tobin JL, and Beales PL (2009) The nonmotile ciliopathies. Genet Med 11, 386–402 [PubMed: 19421068]
4. Brown JM, and Witman GB (2014) Cilia and Diseases. Bioscience 64, 1126–1137 [PubMed: 25960570]
5. Keeling J, Tsiokas L, and Maskey D (2016) Cellular Mechanisms of Ciliary Length Control. Cells 5
6. Mukhopadhyay S, Wen X, Chih B, Nelson CD, Lane WS, Scales SJ, and Jackson PK (2010) TULP3 bridges the IFT-A complex and membrane phosphoinositides to promote trafficking of G protein-coupled receptors into primary cilia. Genes Dev. 24, 2180–2193 [PubMed: 20889716]
7. Fu W, Wang L, Kim S, Li J, and Dynlacht BD (2016) Role for the IFT-A Complex in Selective Transport to the Primary Cilium. Cell reports 17, 1505–1517 [PubMed: 27806291]
8. Picariello T, Brown JM, Hou Y, Swank G, Cochran DA, King OD, Lechtreck K, Pazour GJ, and Witman GB (2019) A global analysis of IFT-A function reveals specialization for transport of membrane-associated proteins into cilia. J. Cell Sci 132
9. Jin H, White SR, Shida T, Schulz S, Aguiar M, Gygi SP, Bazan JF, and Nachury MV (2010) The conserved Bardet-Biedl syndrome proteins assemble a coat that traffics membrane proteins to cilia. Cell 141, 1208–1219 [PubMed: 20603001]
10. Zhang Q, Nishimura D, Seo S, Vogel T, Morgan DA, Searby C, Bugge K, Stone EM, Rahmouni K, and Sheffield VC (2011) Bardet-Biedl syndrome 3 (Bbs3) knockout mouse model reveals common BBS-associated phenotypes and Bbs3 unique phenotypes. Proc. Natl. Acad. Sci. U. S. A 108, 20678–20683 [PubMed: 22139371]
11. Tran PV, Haycraft CJ, Besschetnova TY, Turbe-Doan A, Stottmann RW, Herron BJ, Chesebro AL, Qiu H, Scherz PJ, Shah JV, Yoder BK, and Beier DR (2008) THM1 negatively modulates mouse sonic hedgehog signal transduction and affects retrograde intraflagellar transport in cilia. Nat. Genet 40, 403–410 [PubMed: 18327258]

12. Iomini C, Li L, Esparza JM, and Dutcher SK (2009) Retrograde intraflagellar transport mutants identify complex A proteins with multiple genetic interactions in Chlamydomonas reinhardtii. Genetics 183, 885–896 [PubMed: 19720863]

13. Herron BJ, Lu W, Rao C, Liu S, Peters H, Bronson RT, Justice MJ, McDonald JD, and Beier DR (2002) Efficient generation and mapping of recessive developmental mutations using ENU mutagenesis. Nature genetics 30, 185–189 [PubMed: 11818962]

14. Stottmann RW, Tran PV, Turbe-Doan A, and Beier DR (2009) Ttc21b is required to restrict sonic hedgehog activity in the developing mouse forebrain. Dev. Biol 335, 166–178 [PubMed: 19732765]

15. Tran PV, Talbott GC, Turbe-Doan A, Jacobs DT, Schonfeld MP, Silva LM, Chatterjee A, Prysak M, Allard BA, and Beier DR (2014) Downregulating hedgehog signaling reduces renal cystogenic potential of mouse models. J. Am. Soc. Nephrol 25, 2201–2212 [PubMed: 24700869]

16. Jacobs DT, Silva LM, Allard BA, Schonfeld MP, Chatterjee A, Talbott GC, Beier DR, and Tran PV (2016) Dysfunction of intraflagellar transport-A causes hyperphagia-induced obesity and metabolic syndrome. Dis Model Mech 9, 789–798 [PubMed: 27482817]

17. Davis EE, Zhang Q, Liu Q, Diplas BH, Davey LM, Hartley J, Stoetzel C, Szymanska K, Ramaswami G, Logan CV, Muzny DM, Young AC, Wheeler DA, Cruz P, Morgan M, Lewis LR, Cherukuri P, Maskeri B, Hansen NF, Mullikin JC, Blakesley RW, Bouffard GG, Gyapay G, Rieger S, Tonshoff B, Kern I, Soliman NA, Neuhaus TJ, Swoboda KJ, Kayserili H, Gallagher TE, Lewis RA, Bergmann C, Otto EA, Saunier S, Scambler PJ, Beales PL, Gleeson JG, Maher ER, Attie-Bitach T, Dollfus H, Johnson CA, Green ED, Gibbs RA, Hildebrandt F, Pierce EA, and Katsanis N (2011) TTC21B contributes both causal and modifying alleles across the ciliopathy spectrum. Nat. Genet 43, 189–196 [PubMed: 21258341]

18. Hirano T, Katoh Y, and Nakayama K (2017) Intraflagellar transport-A complex mediates ciliary entry and retrograde trafficking of ciliary G protein-coupled receptors. Mol. Biol. Cell 28, 429–439 [PubMed: 27932497]

19. Zhu B, Zhu X, Wang L, Liang Y, Feng Q, and Pan J (2017) Functional exploration of the IFT-A complex in intraflagellar transport and ciliogenesis. PLoS genetics 13, e1006627 [PubMed: 28207750]

20. Liu W, He X, Yang S, Zouari R, Wang J, Wu H, Kherraf ZE, Liu C, Coutton C, Zhao R, Tang D, Tang S, Lv M, Fang Y, Li W, Li H, Zhao J, Wang X, Zhao S, Zhang J, Arnoult C, Jin L, Zhang Z, Ray PF, Cao Y, and Zhang F (2019) Bi-allelic Mutations in TTC21A Induce Asthenoteratospermia in Humans and Mice. Am J Hum Genet 104, 738–748 [PubMed: 30929735]

21. Pugacheva EN, Jablonski SA, Hartman TR, Henske EP, and Golemis EA (2007) HEF1-dependent Aurora A activation induces disassembly of the primary cilium. Cell 129, 1351–1363 [PubMed: 17604723]

22. Mirvis M, Stearns T, and James Nelson W (2018) Cilium structure, assembly, and disassembly regulated by the cytoskeleton. The Biochemical journal 475, 2329–2353 [PubMed: 30064990]

23. Spalluto C, Wilson DI, and Hearn T (2013) Evidence for reciliation of RPE1 cells in late G1 phase, and ciliary localisation of cyclin B1. FEBS open bio 3, 334–340

24. Phua SC, Chiba S, Suzuki M, Su E, Roberson EC, Pusapati GV, Setou M, Rohatgi R, Reiter JF, Ikegami K, and Inoue T (2017) Dynamic Remodeling of Membrane Composition Drives Cell Cycle through Primary Cilia Excision. Cell 168, 264–279 e215 [PubMed: 28086093]

25. Eguether T, San Agustin JT, Keady BT, Jonassen JA, Liang Y, Francis R, Tobita K, Johnson CA, Abdelhamed ZA, Lo CW, and Pazour GJ (2014) IFT27 links the BBSome to IFT for maintenance of the ciliary signaling compartment. Developmental cell 31, 279–290 [PubMed: 25446516]

26. Liew GM, Ye F, Nager AR, Murphy JP, Lee JS, Aguiar M, Breslow DK, Gygi SP, and Nachury MV (2014) The intraflagellar transport protein IFT27 promotes BBSome exit from cilia through the GTPase ARL6/BBS3. Developmental cell 31, 265–278 [PubMed: 25443296]

27. Corbit KC, Aanstad P, Singla V, Norman AR, Stainier DY, and Reiter JF (2005) Vertebrate Smoothened functions at the primary cilium. Nature 437, 1018–1021 [PubMed: 16136078]

28. Bai CB, Auerbach W, Lee JS, Stephen D, and Joyner AL (2002) Gli2, but not Gli1, is required for initial Shh signaling and ectopic activation of the Shh pathway. Development 129, 4753–4761 [PubMed: 12361967]

29. Mirvis M, Siemers KA, Nelson WJ, and Stearns TP (2019) Primary cilium loss in mammalian cells occurs predominantly by whole-cilium shedding. PLoS biology 17, e3000381 [PubMed: 31314751]

30. Lu H, Toh MT, Narasimhan V, Thamilselvam SK, Choksi SP, and Roy S (2015) A function for the Joubert syndrome protein Arl13b in ciliary membrane extension and ciliary length regulation. Dev. Biol 397, 225–236 [PubMed: 25448689]

31. Driver AM, Shumrick C, and Stottmann RW (2017) Ttc21b Is Required in Bergmann Glia for Proper Granule Cell Radial Migration. J Dev Biol 5

32. Chang CF, Chang YT, Millington G, and Brugmann SA (2016) Craniofacial Ciliopathies Reveal Specific Requirements for GLI Proteins during Development of the Facial Midline. PLoS genetics 12, e1006351 [PubMed: 27802276]

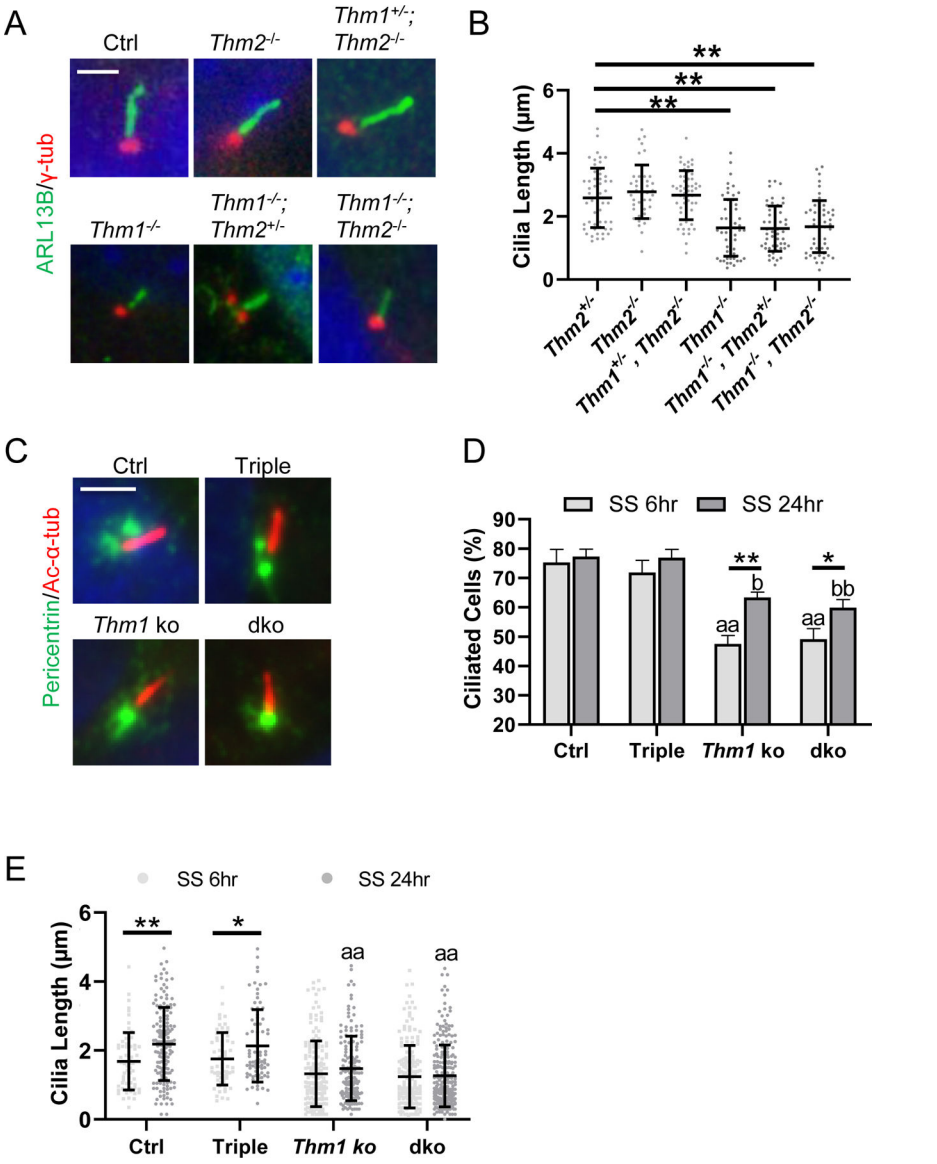

Figure 1. *Thm1* regulates early and late ciliogenesis.

(A) Immunostaining for ARL13B (green) and γ-tubulin (red). Scale bar = 5 μm. (B) Cilia length. 2–3 cell lines per genotype, and ≥40 cilia/genotype were randomly selected per experiment. Each dot represents an individual cilium length. Bars represent mean ± SD. (C) Immunostaining for acetylated α-tubulin (red) and pericentrin (green). Scale bar = 5 μm. (D) Percentage of ciliated MEF and (E) cilia length following 6hr and 24hr serum starvation (SS). Five-to-ten fields were analyzed per condition per experiment, and included ≥ 65 ciliated cells per condition per genotype. Bars represent mean ± SD from 2–3 independent experiments. Statistical significance was determined by ANOVA followed by Tukey's or Dunnett's test. *p<0.05; ** p<0.0001; ^{aa} p<0.0001 compared to Ctrl MEF - 6hr serum starvation; ^{b} p<0.05; ^{bb} p<0.0001 compared to Ctrl MEF - 24hr serum starvation

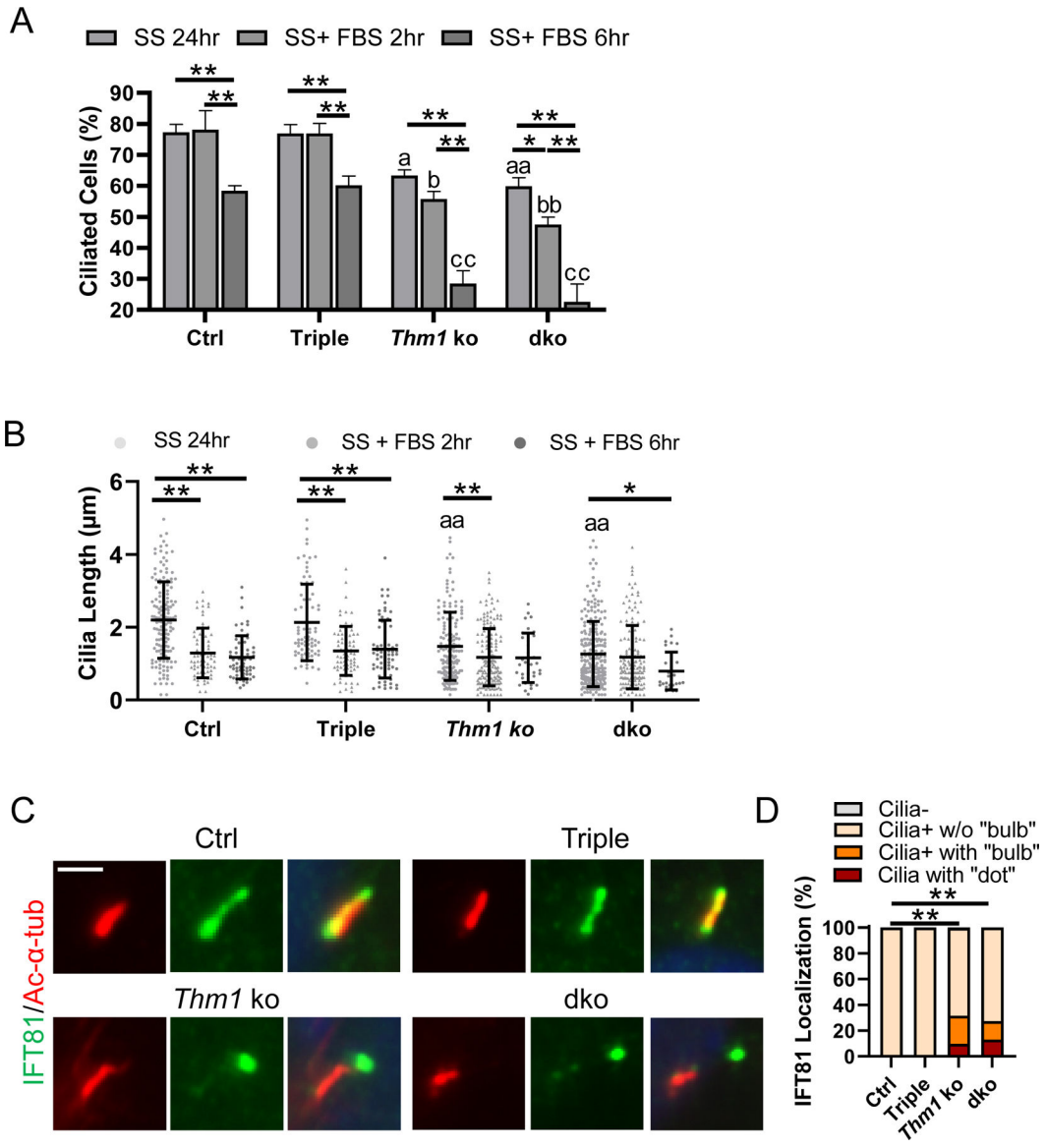

Figure 2. *Thm1* and *Thm2* alter stability of pre-established cilia.

(A) Percentage of ciliated MEF and (B) cilia length after 24hr serum starvation (SS) alone or followed by 2hr or 6 hr FBS restimulation. Five-to-ten fields were analyzed per condition per experiment, and included ≥ 65 ciliated cells per condition per genotype. Bars represent mean ± SD from 2–3 independent experiments. Statistical significance was determined by ANOVA followed by Tukey's or Dunnett's test. *p<0.05; ** p<0.0001; [a] p<0.05; [aa] p<0.0001 compared to Ctrl MEF - 24hr serum starvation; [b] p<0.05; [bb] p<0.0001 compared to Ctrl MEF - 24hr serum starvation + 2hr FBS; [cc] p<0.0001 compared to Ctrl MEF - 24hr serum starvation + 6hr FBS. (C) Immunostaining for IFT81 (green) and acetylated α-tubulin (red) following 24hr serum starvation + 2hr FBS. (D) Quantification of ciliary localization of IFT81, categorized as absent from cilia (Cilia-), present in cilia without a bulbous distal tip (Cilia + w/o bulb), and present in cilia with a bulbous distal tip (Cilia+ with bulb). Stacked bar graphs represent percentage of these occurrences. Total number of Ctrl, Triple,

Thm1 ko and dko cells quantified were 202, 205, 340 and 131, respectively, from 2–3 independent experiments. Statistical significance was determined by χ^2 test. **p<0.0001

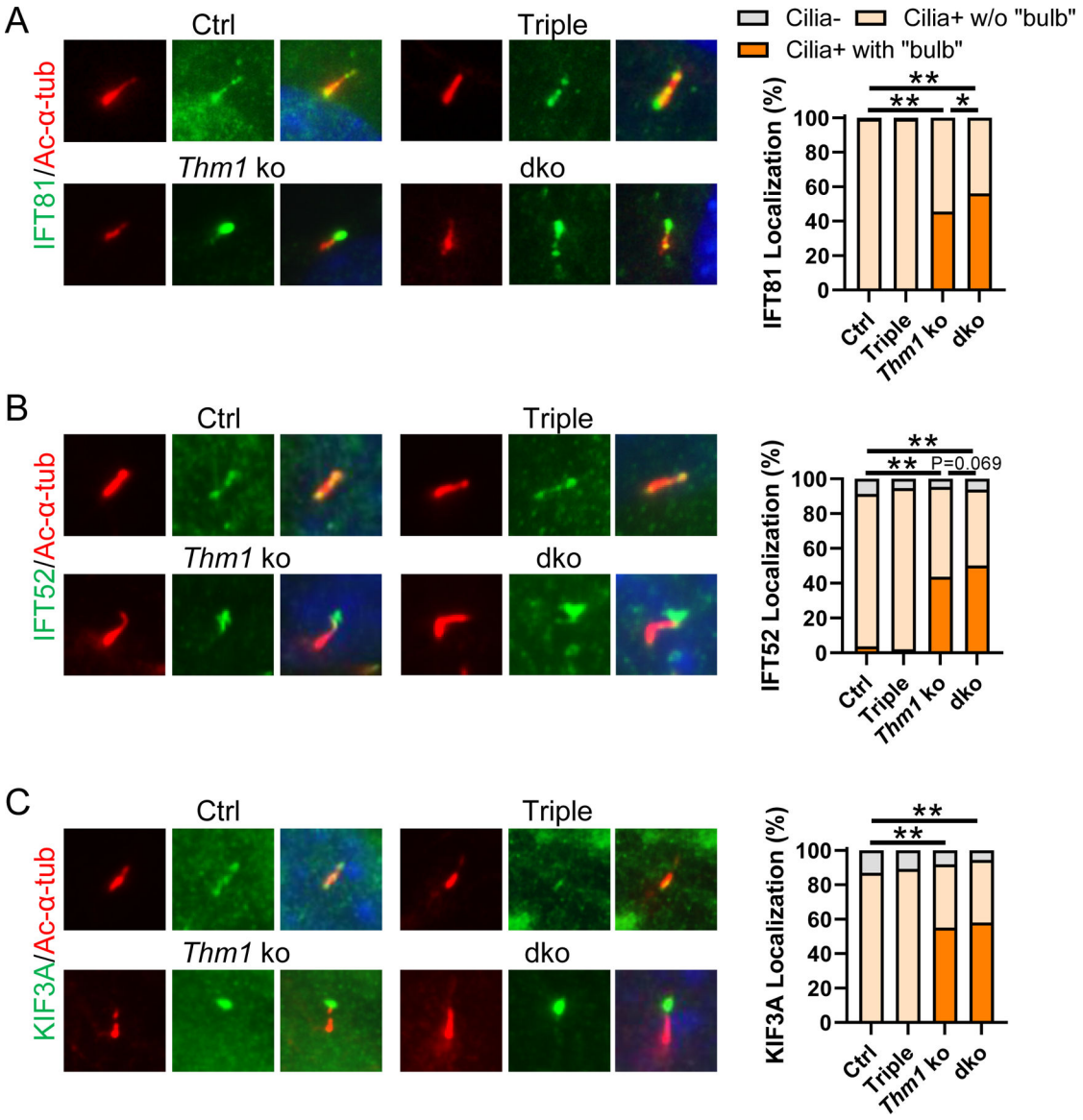

Figure 3. *Thm1* regulates retrograde transport of IFT-B complex.

Immunostaining and quantification for (A) IFT81 (green); (B) IFT52 (green) and (C) KIF3A (green). Ciliary localization of IFT81, IFT52 and KIF3A was categorized as absent from cilia (Cilia-), present in cilia without a bulbous distal tip (Cilia + w/o bulb), and present in cilia with a bulbous distal tip (Cilia+ with bulb). Stacked bar graphs represent percentage of these occurrences. Total number of Ctrl, Triple, *Thm1* ko and dko cells quantified were 150, 151, 200 and 200, respectively, were IFT81; 220, 244, 407 and 408, respectively, for IFT52; were 220, 244, 407 and 408, respectively, for KIF3A, from 2–3 independent experiments. Statistical significance was determined by χ^2 test. *p<0.05; **p<0.0001

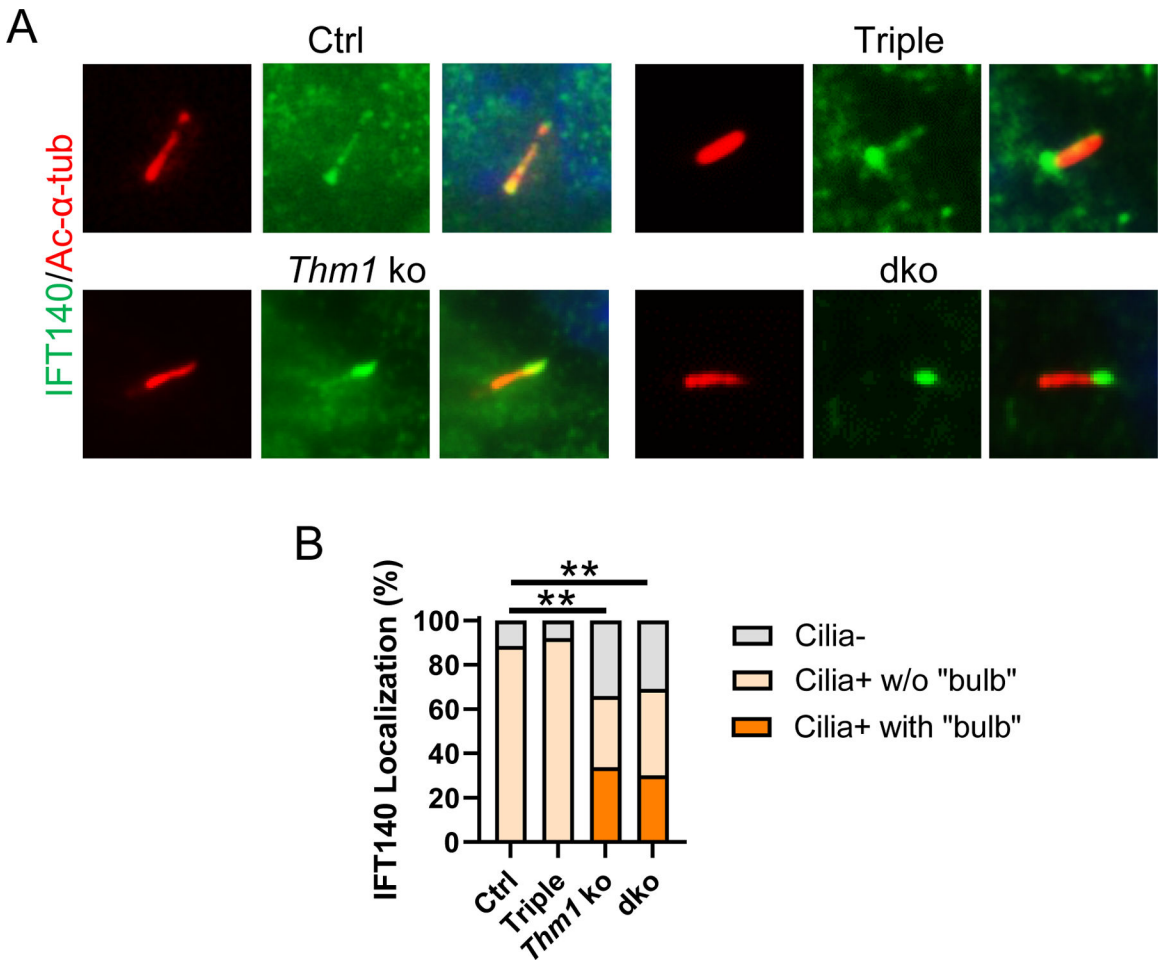

Figure 4. *Thm1* regulates retrograde transport and ciliary entry of IFT-A component, IFT140.
(A) Immunostaining for IFT140 (green) and acetylated-α-tubulin (red). (B) Quantification of IFT140 ciliary localization. Total number of Ctrl, Triple, *Thm1* ko and dko cells quantified were 224, 274, 386 and 385, respectively, from 2–3 independent experiments. Statistical significance was determined by χ^2 test. **p<0.0001

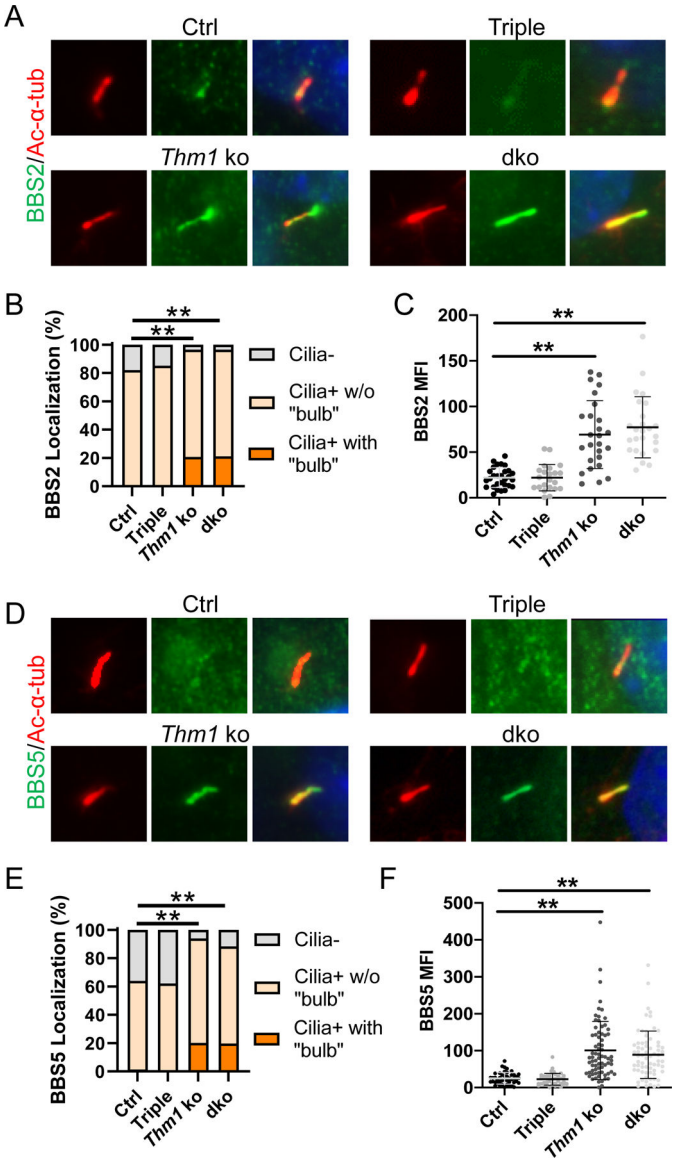

Figure 5. BBSome subunits are increased in *Thm1*-null cilia.

(A) Immunostaining for BBS2 (green) and ac-α-tubulin (red). (B) Quantification of BBS2 ciliary localization. Total number of Ctrl, Triple, *Thm1* ko and dko cells quantified were 183, 167, 334 and 223, respectively, from 2–3 independent experiments. Statistical significance was determined by χ^2 test. (C) Fluorescence intensity of BBS2 in cilia. Each dot represents an individual cilium. Bars represent mean ± SD. Statistical significance was determined by ANOVA followed by Tukey's test. (D) Immunostaining for BBS5 (green) and ac-α-tubulin (red). (E) Quantification of BBS5 ciliary localization. Total number of Ctrl, Triple, *Thm1* ko and dko cells quantified were 219, 261, 229 and 217, respectively, from 3 independent experiments. Statistical significance was determined by χ^2 test. (E) Fluorescence intensity of BBS5 in cilia. Each dot represents an individual cilium. Bars represent mean ± SD. Statistical significance was determined by ANOVA followed by Tukey's test. **p<0.0001

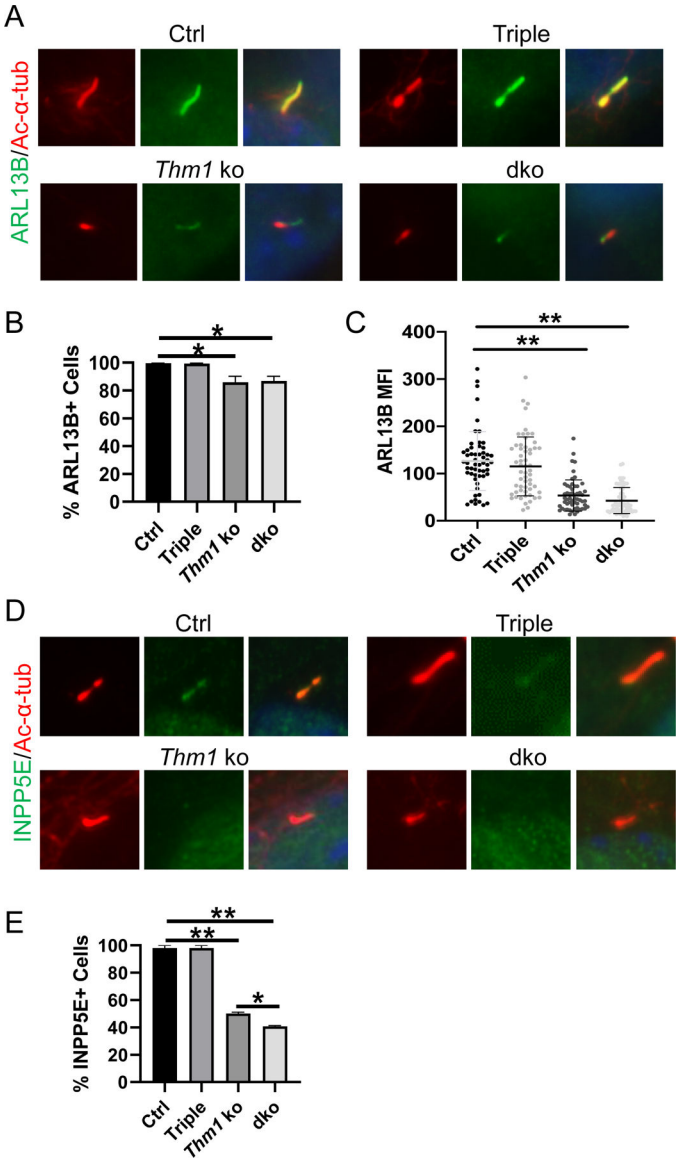

Figure 6. *Thm2* interacts with *Thm1* to mediate ciliary localization of ARL13B and INPP5E.

(A) Immunostaining for ARL13B (green) and ac-α-tubulin (red). (B) Quantification of ARL13B positive cilia. ≥ 150 cells/genotype from 3 independent experiments were quantified. (C) Fluorescence intensity of Arl13b in cilia. Each dot represents an individual cilium. Bars represent mean ± SD. (D) Immunostaining for INPP5E (green) and ac-α-tubulin (red). (E) Quantification of INPP5E positive cilia. ≥ 150 cells/genotype from 3 independent experiments were quantified. Statistical significance was determined by ANOVA followed by Tukey's test. *p<0.05; **p<0.0001

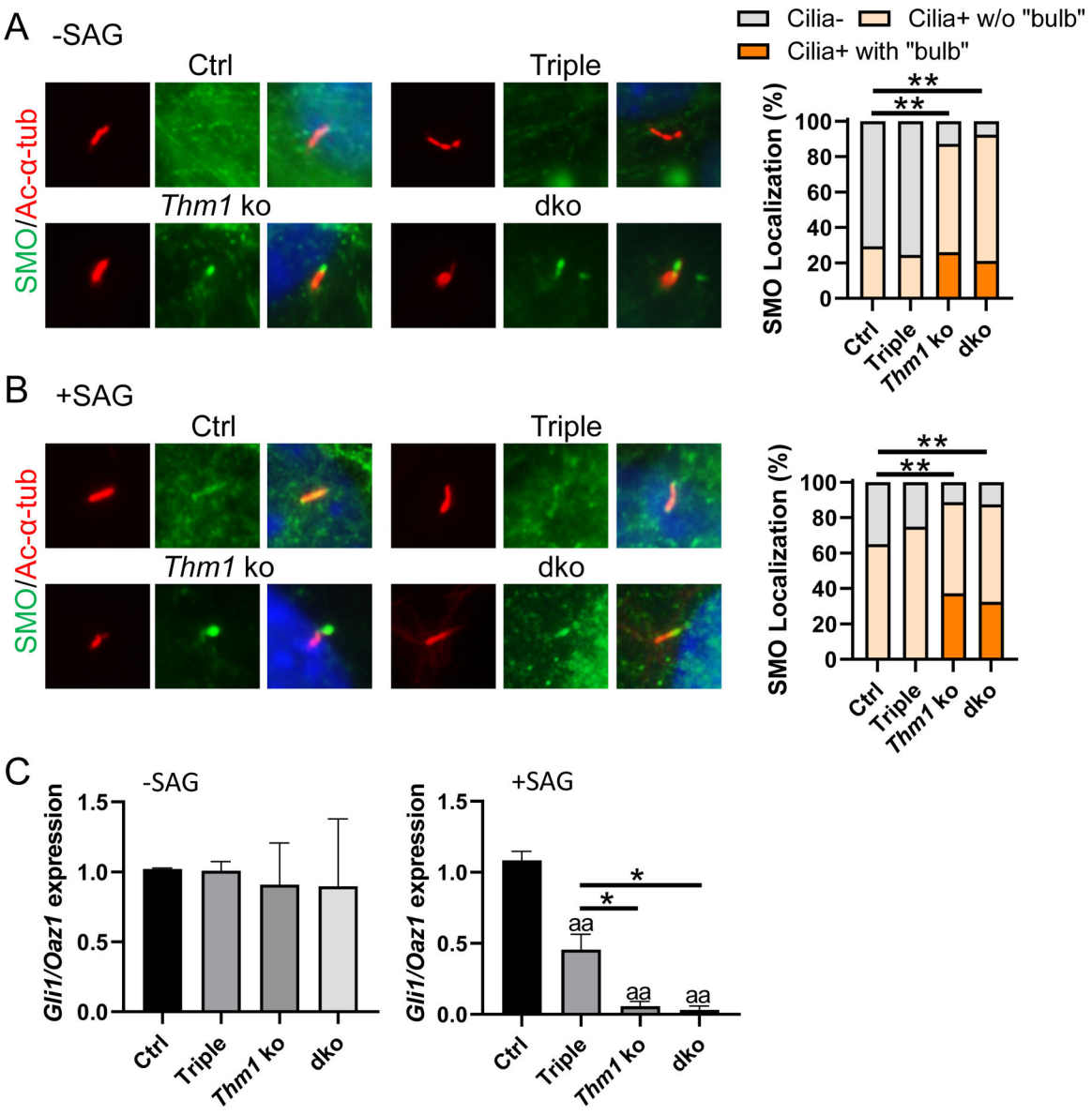

Figure 7. *Thm2* interacts with *Thm1* to regulate Hh signaling.

Immunostaining for SMO and acetylated-α-tubulin of serum-starved MEF treated with (A) DMSO or (B) SAG for 8 hr, with quantification of SMO ciliary localization. Total number of Ctrl, Triple, *Thm1* ko and dko cells quantified in (A) were 191,135, 235 and 223, respectively, and in (B) were 203, 242, 363 and 200, respectively, from 2–3 independent experiments. Statistical significance was determined by χ^2 test. (C) qPCR for *Gli1* on RNA extracts of MEF cultured in 1% FBS overnight, then treated with DMSO or SAG for 48 h in 1% FBS medium. *Gli1/Oaz1* transcript ratios of control cells were set to 1. Graphs represent mean ± SEM. Three MEF lines per genotype were used. Statistical significance was determined by ANOVA followed by Tukey's test. *p<0.05; **p<0.0001; ^{aa} p<0.0001 compared to Ctrl

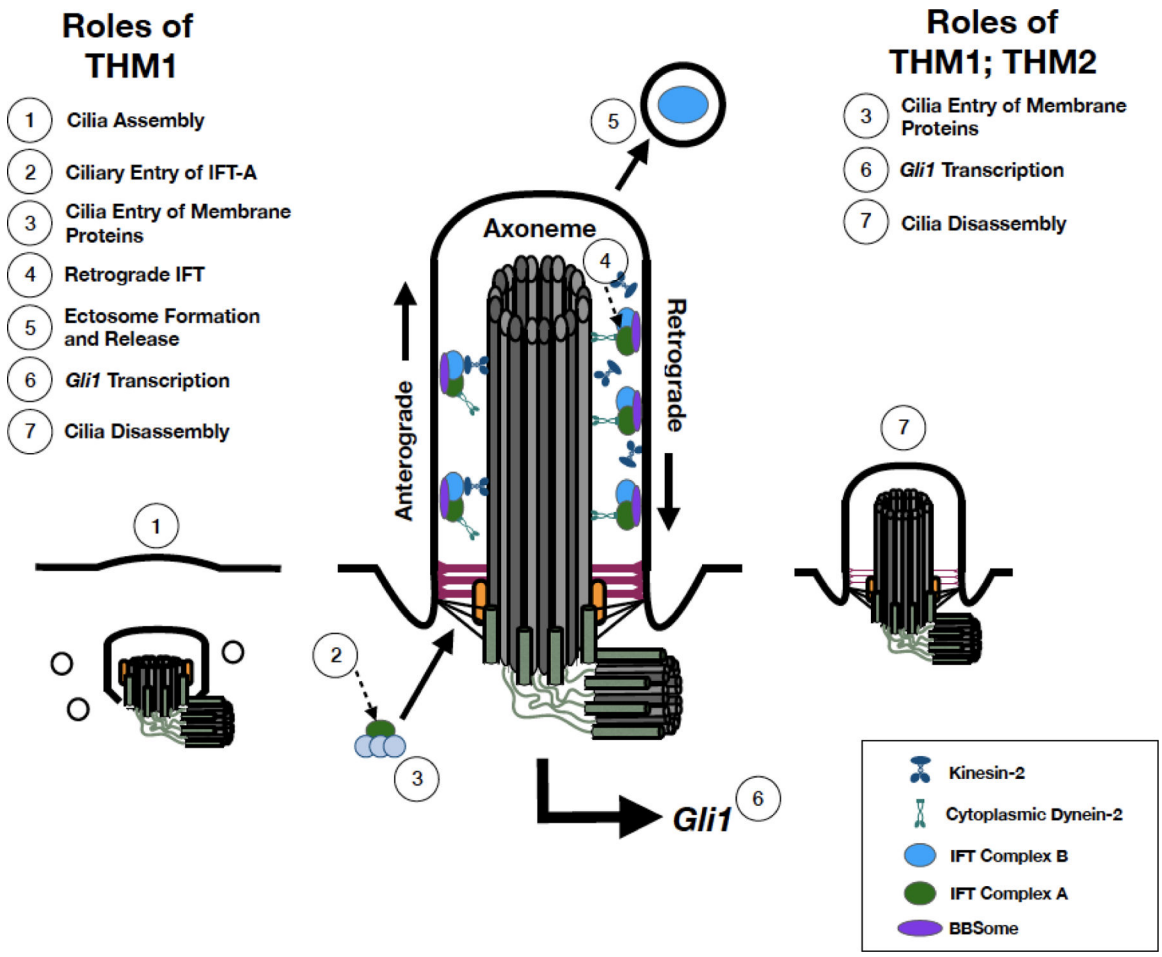

Figure 8. Ciliary roles of *Thm1* and *Thm2*.

Model for *Thm1*, alone and together with *Thm2*, in regulating ciliogenesis, cilia disassembly, ciliary protein trafficking and Hh signaling in MEF.

Table 1.

Frequency of live *Thm1;Thm2* double knock-out embryos

	$Thm1^{aln/+}; Thm2^{\Delta 4-8/+} \times Thm1^{aln/+}; Thm2^{\Delta 4-8/+}$			
	Expected % frequency	**Observed % frequency (no.)**		
Genotype		**E10.5**	**E12.5**	**E14.5**
$Thm1^{aln/aln}$	25	32 (13)	22 (4)	27 (7)
$Thm1^{aln/aln}; Thm2^{\Delta 4-8/+}$	50	46 (19)	44 (8)	69 (18)
$Thm1^{aln/aln}; Thm2^{\Delta 4-8/\Delta 4-8}$	25	22 (9)	33 (6)	4 (1) *

Fisher's Exact Test was applied to analyze differences between expected and observed numbers of *Thm1*-null (including $Thm1^{aln/aln}$ and $Thm1^{aln/aln}; Thm2^{\Delta 4-8/+}$) and *Thm1:Thm2* double knock-out embryos;

* $p<0.05$.